

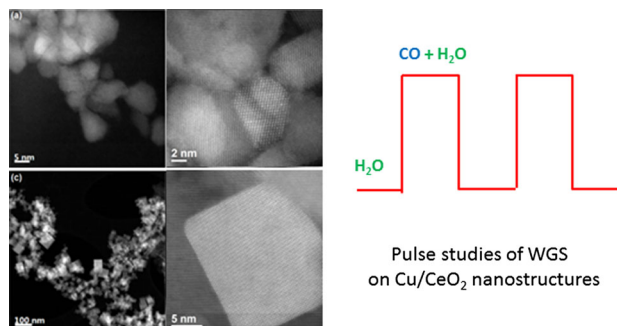
# Pulse Studies to Decipher the Role of Surface Morphology in CuO/CeO<sub>2</sub> Nanocatalysts for the Water Gas Shift Reaction

Fuzhen Zhao · Zongyuan Liu · Wenqian Xu · Siyu Yao · Rui Si ·  
Aaron C. Johnston-Peck · Arturo Martínez-Arias · Jonathan C. Hanson ·  
Sanjaya D. Senanayake · José A. Rodriguez

Received: 4 December 2014 / Accepted: 9 January 2015 / Published online: 23 January 2015  
© Springer Science+Business Media New York 2015

**Abstract** The water-gas shift reaction (WGS,  $\text{CO} + \text{H}_2\text{O} \rightarrow \text{H}_2 + \text{CO}_2$ ) was studied over CuO/CeO<sub>2</sub> catalysts with two different ceria particle morphologies, in the form of nanospheres (ns) and nanocubes (nc). To understand the strong dependence of the WGS reaction activity on the ceria nanoshapes, pulses of CO (without and with water vapor) were employed during in situ X-ray diffraction and X-ray absorption near edge structure measurements done to characterize the catalysts. The results showed that CuO/CeO<sub>2</sub> (ns) exhibited a substantially better activity than CuO/CeO<sub>2</sub> (nc). The higher activity was associated with the unique properties of CuO/CeO<sub>2</sub> (ns), such as the easier reduction of highly dispersed CuO to metallic Cu, the stability of metallic Cu and a larger concentration of Ce<sup>3+</sup> in CeO<sub>2</sub> (ns).

## Graphical Abstract



**Keywords** CuO/CeO<sub>2</sub> · Nanospheres · Nanocubes · Water-gas shift reaction · Transient studies

F. Zhao  
Key Laboratory of Catalysis and Materials Science of the State Ethnic Affairs Commission and Ministry of Education, College of Chemistry and Materials, South-Central University of Nationalities, Wuhan 430074, Hubei, China

F. Zhao · Z. Liu · W. Xu · S. Yao · R. Si ·  
J. C. Hanson · S. D. Senanayake · J. A. Rodriguez (✉)  
Chemistry Department, Brookhaven National Laboratory,  
Upton, NY 11973, USA  
e-mail: rodriguez@bnl.gov

A. C. Johnston-Peck  
Center of Functional Nanomaterials, Brookhaven National  
Laboratory, Upton, NY 11973, USA

A. Martínez-Arias  
Instituto de Catalís Y Petroleoquímica, Consejo Superior de  
Investigaciones Científicas (ICP-CSIC), 28049 Madrid, Spain

## 1 Introduction

The water-gas shift reaction (WGS,  $\text{CO} + \text{H}_2\text{O} \rightarrow \text{H}_2 + \text{CO}_2$ ) has become one of the most important processes in the chemical industry for the production of clean molecular hydrogen for proton exchange membrane fuel cells (PEMFCs) [1]. As the reaction is exothermic ( $\Delta H = -41.1$  kJ/mol) [2] and equilibrium limited, a high conversion of CO can be obtained with a two-stage process: a high temperature shift (350–500 °C) using mixtures of Fe–Cr oxides as catalysts and a low temperature shift (200–250 °C) with Zn–Al–Cu oxides as catalysts [3]. However, the current industrial catalysts for the WGS reaction are not appropriate for use with fuel cells, particularly in mobile systems, due to the problems related to their narrow temperature regime of operation and

pyrophoric characteristics, as well as the requirement of lengthy and complex activation steps before usage [4]. Great attempts have been made in recent years to seek WGS catalysts with high activity, stability, free of pre-treatment requirements, that operate at lower temperatures.

Precious metal catalysts, such as Pt, Pd, Ru and Au, have been widely studied for the WGS reaction and have showed high catalytic activity and stability at low temperatures [5]. However, the high cost and the limited abundance of the precious metals inhibits their application and has encouraged researchers to look for base metal catalysts.

In recent years, cerium oxide has received considerable attention due to its unique reducibility properties and oxygen storage capability (OSC) [6]. This reducibility of CeO<sub>2</sub> can be significantly enhanced by the presence of a small amount of a transition metal, for instance the CuO/CeO<sub>2</sub> system. Because of its high oxygen storage capacity, strong metal-support interactions and facility to generate oxygen vacancies [7], CuO/CeO<sub>2</sub> catalyst has been widely applied in many catalytic processes including: selective catalytic reduction of NO with NH<sub>3</sub> [8] or C<sub>3</sub>H<sub>6</sub> [9], selective oxidation of CO in excess hydrogen [10] and the WGS reaction [11]. Recently, it has been recognized that the morphology of CeO<sub>2</sub> strongly influence the surface atom densities, electronic structure, and chemical reactivity of this oxide [12]. Therefore, many studies of CeO<sub>2</sub> systems have focused on the shape-dependent properties. Meher and Rao [12] synthesized highly uniform CeO<sub>2</sub> nanorods and nanoflowers and tested for their soot oxidation activity. They found that the CeO<sub>2</sub> sample with nanorod morphology was more active due to larger CeO<sub>2</sub>/soot interface than the CeO<sub>2</sub> sample with nanoflower morphology. Shen and co-workers [13] studied the catalytic activities of ceria nanowires, nanorods and nanoparticles for CO oxidation. It was found that nanowires expose a large proportion of active planes on the surface, resulting in a much higher activity than the others. Previously, we reported three CuO/CeO<sub>2</sub> catalysts with different morphologies of ceria, namely nanospheres, nanorods and nanocubes, and investigated their catalytic performance for the WGS reaction [14]. The results showed that nanosphere ceria catalysts were more preferable than the other two types, due to their excellent water dissociation capability, the best dispersion of Cu and a strong Cu–CeO<sub>x</sub> interaction [14].

Pulse or transient experiments can provide more dynamic details than steady-state measurements. They have been widely used in many catalytic studies to reveal details of the reaction mechanism [15, 16]. In this study, we use the pulse method to investigate the relationship between ceria morphology (nanospheres and nanocubes) and catalytic activity, hoping to gain further insight to

understand the performance of the CuO/CeO<sub>2</sub> catalysts and how their components respond to CO and water.

## 2 Experimental

### 2.1 Catalysts Preparation

The ceria nanospheres were synthesized by a reverse microemulsion method containing n-Heptane, Triton-X-100 and n-Hexanol in amounts similar to those reported previously [3]. The required amount of ceria nitrate was dissolved in distilled water and dispersed within the previously mentioned organic components to form a reverse microemulsion. After 1 h stirring of the microemulsion, a (tetramethyl ammonium hydroxide) TMAH-containing solution was added to the cerium-containing solution and it was left for the period of 24 h in order to complete the precipitation reaction. The resulting solid was then separated by centrifugation and decantation; rinsed with methanol; dried overnight at 100 °C and finally calcined at 500 °C for 2 h in air. Ceria nanocubes were synthesized by a hydrothermal method. The cerium nitrate precursor was dissolved in a NaOH aqueous solution with stirring. The mixture was introduced into a stainless steel autoclave and kept at 180 °C for 24 h. The precipitants were further separated, washed and dried at 60 °C overnight and the resulting powder was calcined at 500 °C for 2 h in air. Copper based catalysts, employing the as-prepared CeO<sub>2</sub> supports, were synthesized by incipient wetness impregnation using copper nitrate as the precursor (5 wt% Cu loading). The samples were dried overnight at 100 °C and then calcined in air at 500 °C for 2 h. The above as-prepared catalysts are labeled as CuO/CeO<sub>2</sub> (ns) and (nc) for the nanosphere and nanocube ceria supports, respectively. Specific surface areas ( $S_{\text{BET}}$ ), as determined from N<sub>2</sub> adsorption isotherms, were of 72 and 29 m<sup>2</sup>/g for CuO/CeO<sub>2</sub> (ns) and (nc) catalysts, respectively. Annular dark field STEM (Fig. 1) showed that ceria nanocubes primarily expose (100) faces, with (110) terminations at the corners, and ceria nanospheres were dominated by (111) faces but in some cases the particles were irregular without well-defined facets [14]. CuO particles were not resolvable from TEM and STEM images mainly due to the low contrast between Cu and Ce, and the high dispersion of very small particles [14].

### 2.2 XRD

XRD was performed at beamline X7B ( $\lambda = 0.3196 \text{ \AA}$ ) of the National Synchrotron Light Source (NSLS) at Brookhaven National Laboratory (BNL). The flow cell system was the same as in the reaction activity experiments as

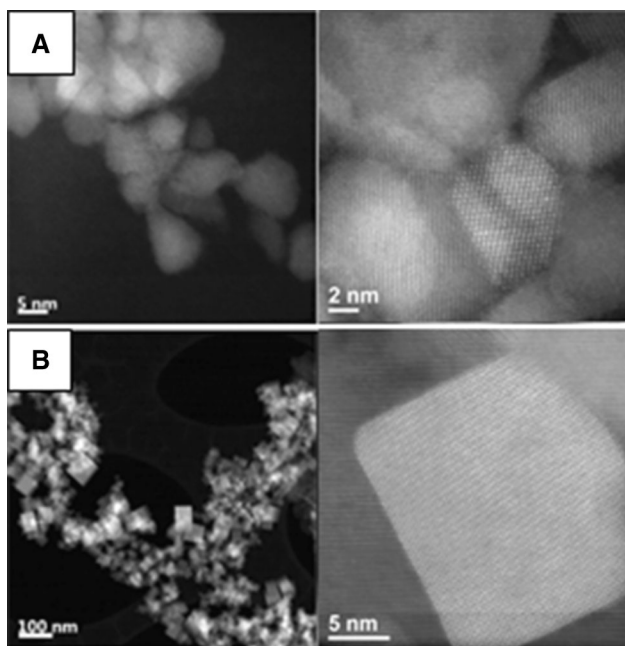


**Fig. 1** STEM and high-resolution STEM images of CuO/CeO<sub>2</sub> (ns) (a) and CuO/CeO<sub>2</sub> (nc) (b) catalysts

described in Sect. 2.4. Two-dimensional transmission diffraction data were collected with a PerkinElmer amorphous silicon detector, and the powder diffraction rings were subsequently integrated with the program Fit2D [17] to obtain XRD profiles (intensity vs.  $2\theta$ ). The instrument parameters were derived from the fit of a LaB<sub>6</sub> reference pattern. Lattice parameters and phase fractions were determined by Rietveld refinement using the program GSAS (General Structure Analysis System).

### 2.3 XANES

Cu K edge in situ XANES were collected at beamline X19A of the NSLS at BNL. The flow cell system was the same as in the reaction activity experiments, except that the sample was loaded into a Kapton capillary. The X-ray absorption spectra were taken repeatedly in the “fluorescence yield mode” using a passivated implanted planar silicon (PIPS) detector cooled with circulating water. The XANES data were then analyzed using the Athena program.

### 2.4 WGS Activity Experiment

WGS reaction activity experiments were performed in a quartz capillary (0.9 mm i.d.) mounted in a flow cell system described previously [15, 18]. 2–3 mg of the sample were loaded between two quartz wool beds at atmospheric pressure. A resistance heating coil was used to heat the sample capillary, and the catalyst temperature was monitored with a K-type thermocouple placed inside the capillary in the

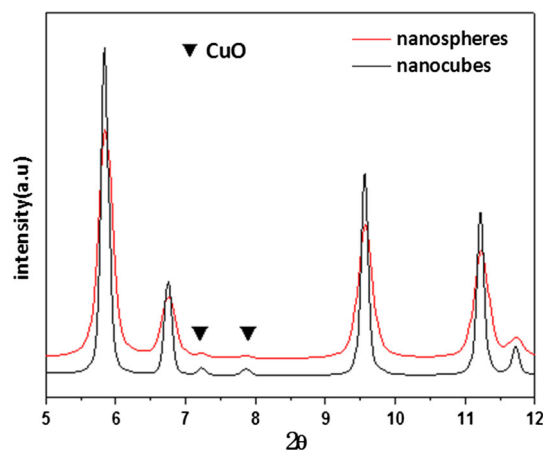
vicinity of the catalyst bed. In a set of initial experiments, the samples were exposed to CO or water alone. This was followed by a study of the behavior of the catalysts under a mixture of CO and water. CO was pulsed for periods of 25 min, while the flow of H<sub>2</sub>O was kept constant. The total feed gas mixture typically contained 1 % CO and/or 3 % H<sub>2</sub>O in helium with a flow rate of 10 mL/min. The outlet products were measured with a calibrated quadrupole mass spectrometer. During the studies with pulses, the temperature of the sample was maintained at 250 or 400 °C.

## 3 Results and Discussion

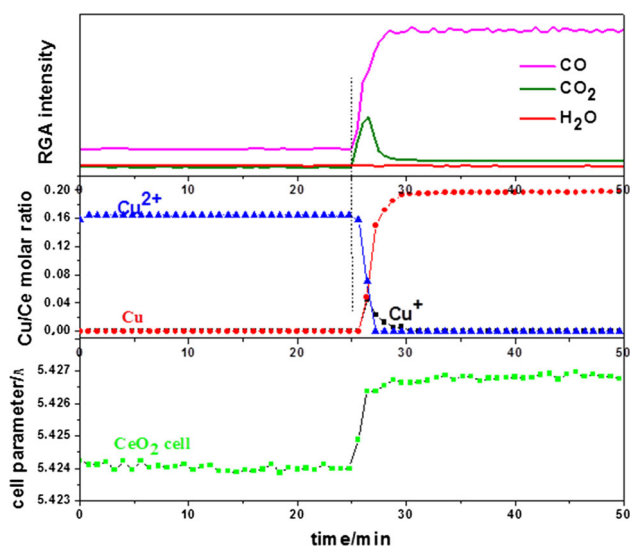
### 3.1 CO Reduction Experiments on CuO/CeO<sub>2</sub> (nc) and CuO/CeO<sub>2</sub> (nc) Catalysts

Figure 2 displays XRD patterns for the as-prepared CuO/CeO<sub>2</sub> (nc) and CuO/CeO<sub>2</sub> (ns) catalysts at room temperature. One can see strong diffraction lines for CeO<sub>2</sub> and small features for CuO. The loading of Cu was similar in both cases (~5 wt%). From Rietveld refinement of these XRD data one can get CuO/CeO<sub>2</sub> molar ratios of 0.16 for CuO/CeO<sub>2</sub> (nc) and 0.08 for CuO/CeO<sub>2</sub> (ns). In the case of the CuO/CeO<sub>2</sub> (ns) sample, it is known that a significant part of the copper oxide is in an amorphous phase not seen by XRD but observed in measurements of X-ray absorption spectroscopy at the Cu K-edge [14]. On the other hand, almost all the CuO present in the CuO/CeO<sub>2</sub> (nc) sample is in a crystalline phase [14].

Reduction experiments with a pulse of CO ( $T = 250$  °C) were performed to evaluate the redox properties of CuO and CeO<sub>2</sub> in the two catalysts. Results are shown for the CuO/CeO<sub>2</sub> (nc) sample in Fig. 3 combining measurements of mass spectrometry at the outlet of

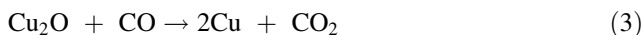
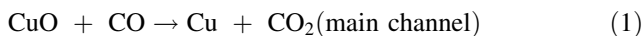


**Fig. 2** Diffraction patterns for the CuO/CeO<sub>2</sub> (ns) and CuO/CeO<sub>2</sub> (nc) catalysts



**Fig. 3** In situ XRD: reduction of a CuO/CeO<sub>2</sub> (nc) catalyst under a pulse of CO at 250 °C

the reactor (RGA intensities for CO and CO<sub>2</sub>) and the analysis of in situ time-resolved XRD data. As CO was pulsed into the reactor, the CuO phase transformed to metallic Cu very quickly and only a little Cu<sup>+</sup> was detected by the XRD measurement.



Most of the transformation occurred within 5 min of the introduction of CO into the reactor. At the same time that there was an almost complete reduction of CuO, and we found a partial reduction of the ceria with a small expansion of the ceria lattice parameter (Ce<sup>3+</sup> is bigger than Ce<sup>4+</sup>) [19].



The ceria lattice parameter changed from 5.424 Å (when the flow did not contain CO) to 5.427 Å (when CO was introduced). In Fig. 3, the consumption of CO stops almost at the same time that the signals for metallic copper and the ceria lattice parameter reach a constant value. This indicates that in the transient period, there is a strong link between the reduction of CuO<sub>y</sub> and CeO<sub>x</sub> (i.e. the transformations in Eqs. (1)–(4) take place simultaneously). This is somewhat surprising, since bulk ceria has a larger stability than copper oxides. Thus, it is likely that the Ce<sup>4+</sup> sites reduced upon exposure of CuO/CeO<sub>2</sub> (nc) to CO were probably associated with a CuO–CeO<sub>2</sub> interface.

Figures 4 and 5 show data of in situ XRD and XANES for the exposure of a CuO/CeO<sub>2</sub> (ns) catalyst to a pulse of CO at 250 °C, respectively. As mentioned above, this system contained almost equal fractions of crystalline and

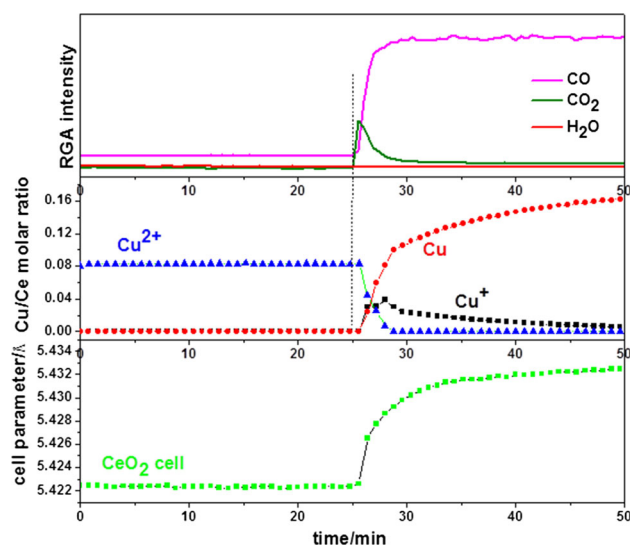


**Fig. 4** In situ XRD: reduction of a CuO/CeO<sub>2</sub> (ns) catalyst under a pulse of CO at 250 °C

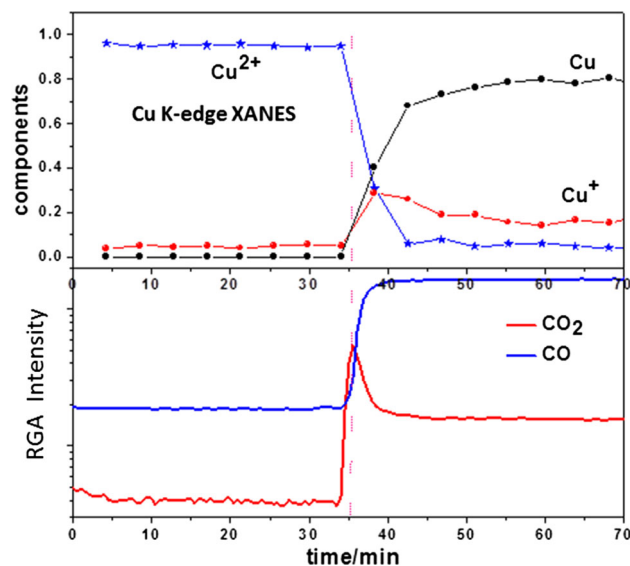


**Fig. 5** In situ XANES: reduction of a CuO/CeO<sub>2</sub> (ns) catalyst under a pulse of CO at 250 °C

amorphous CuO [14] and for that reason was also studied with XANES. Both sets of results indicate that Eqs. (1)–(4) occur during the reduction of the CuO/CeO<sub>2</sub> (ns) sample. Most of the transformations take place in the first 5 min of reaction. An important difference with respect to CuO/CeO<sub>2</sub> (nc) is in the stability of the formed Cu<sup>+</sup>. In the case of CuO/CeO<sub>2</sub> (ns), a substantial fraction of the Cu<sup>+</sup> generated is not a transient species and remains in the sample after exposure to CO for a period of 25 min. This is interesting because bulk Cu<sub>2</sub>O is not stable in an atmosphere of CO at 250 °C [14, 18, 20]. The extra stability of Cu<sup>+</sup> is probably a consequence of the existence of strong Cu<sub>2</sub>O ↔ CeO<sub>y</sub> interactions on the ceria (ns) support. The

similar trends seen in Fig. 4 for the increase in the amount of metallic Cu formed and the expansion of the ceria lattice indicate that CO reduces  $\text{Cu}^{2+}$  and  $\text{Ce}^{4+}$  cations present in a CuO– $\text{CeO}_2$  interface, as was also seen for the CuO/ $\text{CeO}_2$  (nc) sample. Furthermore, a comparison of the results in Figs. 3 and 4 shows a larger  $\text{CeO}_2$  cell expansion for CuO/ $\text{CeO}_2$  (ns) than for CuO/ $\text{CeO}_2$  (nc), which implies the formation of more oxygen vacancies in the CuO/ $\text{CeO}_2$  (ns) catalysts.

### 3.2 Exposure of CuO/ $\text{CeO}_2$ (nc) and CuO/ $\text{CeO}_2$ (ns) Catalysts to Water

When the CuO/ $\text{CeO}_2$  (nc) and CuO/ $\text{CeO}_2$  (ns) samples were exposed to pulses of water at 250 °C, we observed no changes in the XRD patterns.

### 3.3 WGS Activity of CuO/ $\text{CeO}_2$ (nc) and CuO/ $\text{CeO}_2$ (ns) Catalysts and the Pulsing of CO Under a Water Environment

Figure 6 shows data for the production of hydrogen over CuO/ $\text{CeO}_2$  (nc) and CuO/ $\text{CeO}_2$  (ns) catalysts through the WGS at temperatures between 200 and 400 °C. Both materials become catalytically active at temperatures above 200 °C [14]. CuO/ $\text{CeO}_2$  (ns) is always a better catalyst than CuO/ $\text{CeO}_2$  (nc), and the gap in catalytic activity increases when the temperature is raised. Previous experiments of in situ DRIFTS showed that these two catalysts exhibited infrared spectra with different line-shapes in the region between 1,700 and 800  $\text{cm}^{-1}$  [14]. The different morphologies of the catalysts (Fig. 1) led to different types of adsorbed carbonates. CuO/ $\text{CeO}_2$  (nc) showed two strong

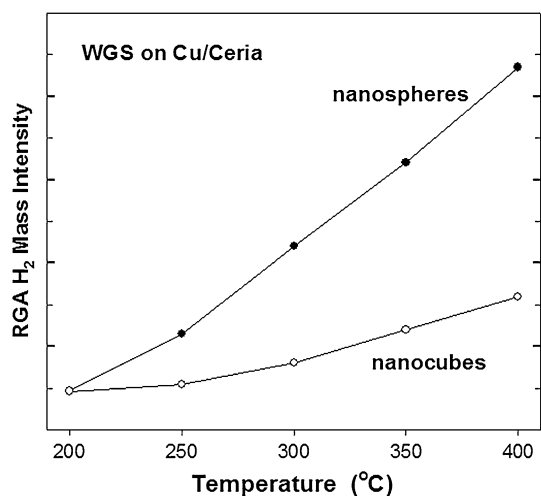


**Fig. 6** Production of hydrogen during the WGS over CuO/ $\text{CeO}_2$  (ns) and CuO/ $\text{CeO}_2$  (nc) catalysts. The feed gas mixture contained 1 % CO and 3 %  $\text{H}_2\text{O}$  in helium with a flow rate of 10 mL/min

bands centered at 1,466 and 1,394  $\text{cm}^{-1}$  associated with carbonates adsorbed on the (100) face [14]. These bands were not seen on the CuO/ $\text{CeO}_2$  (ns) catalyst and were present on CuO/ $\text{CeO}_2$  (nc) at a wide range of temperature. These carbonate species were strongly bound to the nanocubes and do not participate in the catalytic process [14]. They may poison the active sites on the surface of CuO/ $\text{CeO}_2$  (nc) [14]. In this article, we examine how CuO/ $\text{CeO}_2$  (nc) and CuO/ $\text{CeO}_2$  (ns) respond to the pulsing of CO under a water environment. The sample was kept at a temperature of 250 °C when the onset of  $\text{H}_2$  production appears in Fig. 6.

Figure 7 displays in situ XRD results collected after exposing CuO/ $\text{CeO}_2$  (nc) to pulses of CO under a constant flow of water at 250 °C. As soon as CO was added to the water, there was a fast reduction of  $\text{Cu}^{2+}$  to Cu and an expansion of the ceria lattice due to the formation of some  $\text{Ce}^{3+}$ . The amount of  $\text{Cu}^+$  formed as an intermediate was small and disappeared fast. After 2–3 min of the CO pulse, the system reached a steady state with  $\text{Cu/CeO}_{2-x}$  as the active phase of the catalyst and  $\text{H}_2$  and  $\text{CO}_2$  evolving into gas phase. The magnitude of the change in the ceria lattice after exposure to the CO/ $\text{H}_2\text{O}$  mixture (Fig. 7) was comparable to the magnitude seen upon exposure to CO alone (Fig. 3). The removal of the CO gas from the feed to the reactor ( $t = 50$ –60 min, Fig. 7) produced drastic changes in the chemical state of the catalyst. As soon as the amount of CO present in the reactor was reduced, the water started to reoxidize the  $\text{Ce}^{3+}$  sites to  $\text{Ce}^{4+}$  with a contraction in the lattice of ceria

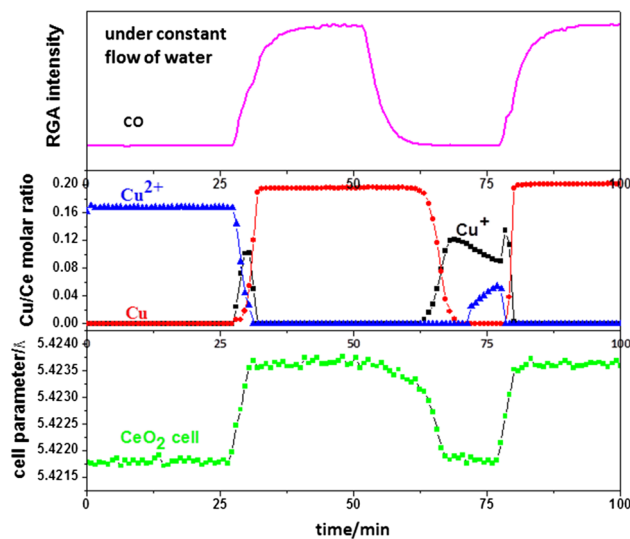
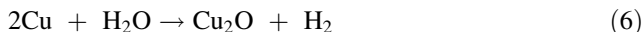


**Fig. 7** In situ XRD results for a CuO/ $\text{CeO}_2$  (nc) catalyst under WGS reaction conditions at 250 °C. The sample was under a constant flow of water and the CO was pulsed as indicated. Under WGS reaction conditions, the feed gas mixture typically contained 1 % CO and/or 3 %  $\text{H}_2\text{O}$  in helium with a flow rate of 10 mL/min



Eventually, the metallic Cu reacts with water to form Cu<sup>1+</sup> and Cu<sup>2+</sup> cations in a sequential way



These results clearly show that the active Cu/CeO<sub>2-x</sub> (nc) phase under WGS conditions is not stable under oxidizing conditions. However, upon a second pulse of CO (t > 80 min), there is a very fast reduction of CuO, Cu<sub>2</sub>O and CeO<sub>2</sub> to yield the active Cu/CeO<sub>2-x</sub> (nc) phase under WGS conditions.

Figure 8 shows the data for the pulsing of CO, under a constant flow of water, over a CuO/CeO<sub>2</sub> (ns) catalyst at 250 °C. As soon as CO is introduced into the reactor (t > 28 min), one sees a fast reduction of Cu<sup>2+</sup> to eventually produce metallic Cu and an expansion of the ceria lattice as a consequence of the formation of some Ce<sup>3+</sup>. Interestingly, the amount of Cu<sup>1+</sup> formed is smaller and less stable than seen after exposing the catalyst to pure CO (Figs. 4 and 5). A similar phenomenon has been observed for an inverse CeO<sub>x</sub>/CuO catalyst [7] and seems to go against the changes in oxidation state predicted by Eqs. (6) and (7). In principle, the water could modify the Cu<sub>2</sub>O–CeO<sub>y</sub> interactions to facilitate the reduction of Cu<sup>1+</sup> by CO [7]. It could also help to remove carbonates formed on CuO/CeO<sub>2</sub> (ns) upon exposure to CO that prevent a full reduction of copper [7]. In any case, the active phase for the WGS on CuO/CeO<sub>2</sub> (ns) and CuO/CeO<sub>2</sub> (nc) involves

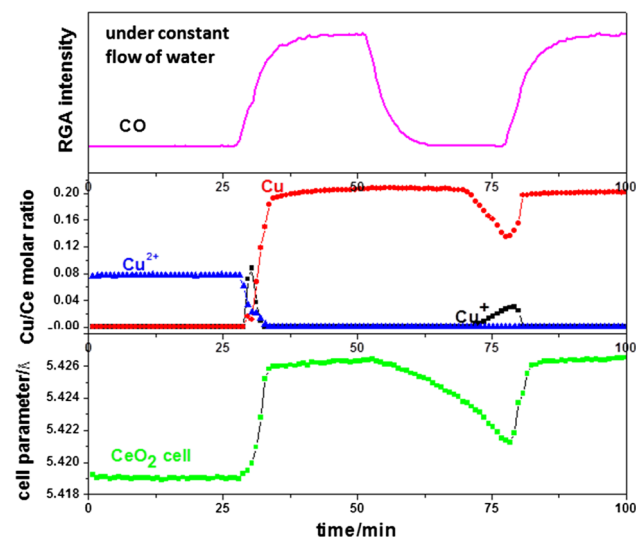


**Fig. 8** In situ XRD results for a CuO/CeO<sub>2</sub> (ns) catalyst under WGS reaction conditions at 250 °C. The sample was under a constant flow of water and the CO was pulsed as indicated. Under WGS reaction conditions, the feed gas mixture typically contained 1 % CO and/or 3 % H<sub>2</sub>O in helium with a flow rate of 10 mL/min

metallic copper on partially reduced ceria. Comparing the expansion of the ceria lattice in Figs. 7 and 8, it appears that the amount of Ce<sup>3+</sup> formed is larger on the CuO/CeO<sub>2</sub> (ns) catalyst.

In Fig. 8, the removal of CO from the feed to the reactor (t > 53 min) starts a slow contraction of the ceria lattice produced by the disappearance of Ce<sup>3+</sup> centers as a consequence of the reoxidation of ceria by water, Eq. (5). For a while (~20 min), there is no reoxidation of metallic Cu into Cu<sup>1+</sup> [i.e. no reaction (6)]. A comparison of the results in Figs. 7 and 8 indicates that the active phase of the CuO/CeO<sub>2</sub> (ns) catalyst is less sensitive to reoxidation by water than that of the CuO/CeO<sub>2</sub> (nc) catalyst. This is probably a consequence of stronger Cu ↔ CeO<sub>x</sub> interactions in the CuO/CeO<sub>2</sub> (ns) system and correlates with its higher activity for the WGS (Fig. 6). The introduction of a second pulse of CO in Fig. 8 (t > 78 min) produces a fast reduction of Cu<sup>1+</sup> and the reoxidized ceria; in less than 2 min the catalyst adopts its active Cu/CeO<sub>2-x</sub> configuration.

As mentioned above, a comparison of the results in Figs. 7 and 8 indicates that the expansion of the ceria lattice in CuO/CeO<sub>2</sub> (ns) is larger than in CuO/CeO<sub>2</sub> (nc). The same trend was found in experiments done at 400 °C, see Fig. 9. An increase in temperature leads to a larger reduction of both ceria supports but the concentration of Ce<sup>3+</sup> sites is always larger for the CuO/CeO<sub>2</sub> (ns) system. This is important since the Ce<sup>3+</sup> centers are associated with the dissociation of water and the production of H<sub>2</sub> [19, 20]. Clearly, the higher the concentration of Ce<sup>3+</sup>, the greater the catalytic activity for H<sub>2</sub> production as indicated by a comparison of Figs. 6 and 9.

The reasons for the good performance on CuO/CeO<sub>2</sub> catalysts have been studied before. Ozkan and co-workers [21] investigated the effect of support morphology and impregnation medium on the activity of Cu/CeO<sub>2</sub> catalysts

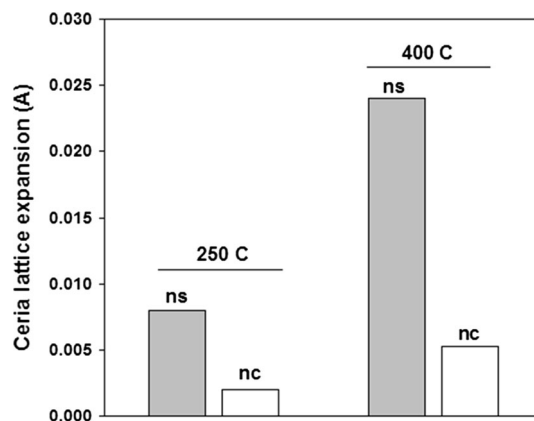


**Fig. 9** Expansion in the ceria lattice at 250 and 400 °C for CuO/CeO<sub>2</sub> (ns) and CuO/CeO<sub>2</sub> (nc) catalysts under WGS reaction conditions. The feed gas mixture contained 1 % CO and 3 % H<sub>2</sub>O in helium with a flow rate of 10 mL/min

in the WGS reaction. They concluded that the finely dispersed copper species constitute the active sites for the WGS reaction. Yoon and co-workers [11] reported Cu–CeO<sub>2</sub> catalyst prepared by a co-precipitation method and mainly ascribed the outstanding catalytic performance of 80 wt%Cu–CeO<sub>2</sub> catalyst to Cu sintering resistance, resulting from a strong interaction between Cu and CeO<sub>2</sub>. According to the results of our experiments, the better activity of CuO/CeO<sub>2</sub> (ns) may be associated with the following three factors.

In the first place, the easy reduction of highly dispersed CuO to metallic Cu is a very important factor for the high activity. In the CuO/CeO<sub>2</sub> (ns) sample, about half of the CuO particles are in the highly dispersed state, while almost all the CuO is in the crystalline form on CuO/CeO<sub>2</sub> (nc) [14]. It has been well documented that the finely dispersed CuO has a reduction temperature much lower than that of the bulk CuO [22, 23]. Since metallic Cu is commonly accepted as the active phase for the WGS reaction [24], it is no strange that CuO/CeO<sub>2</sub> (nc) sample has a lower activity than CuO/CeO<sub>2</sub> (ns).

Second, the stability of metallic Cu is another key factor. The metallic Cu seems very easy to be oxidized on CuO/CeO<sub>2</sub> (nc), see Fig. 7. H<sub>2</sub>O can oxidize Cu to Cu<sup>+</sup> and further to Cu<sup>2+</sup> (Fig. 7). On the contrary, the metallic Cu is rather stable on CuO/CeO<sub>2</sub> (ns), only a small extent to reoxidation to Cu<sup>+</sup> can be observed (Fig. 8). The different stability of metallic Cu can be ascribed to the mobility of oxygen in ceria. Overbury and co-workers [25] found that the oxygen mobility on CeO<sub>2</sub> nanocubes is much higher than that on CeO<sub>2</sub> octahedra (nanosphere in our experiment since they have predominantly the same (111) face). The relative freedom for the movement of oxygen facilitated the oxidation of the metallic Cu on CeO<sub>2</sub> nanocubes. Therefore, Cu on CuO/CeO<sub>2</sub> (nc) exhibits a poorer stability than on CuO/CeO<sub>2</sub> (ns), leading to a lower activity.

Third, CeO<sub>2</sub> (ns) has a larger concentration of O vacancies and Ce<sup>3+</sup>, Fig. 9. These oxygen vacancies can act as sites for the dissociation of H<sub>2</sub>O molecules to form OH groups or H<sub>2</sub> and O<sup>2-</sup> anions, a rate-limiting step independent of the reaction mechanism [26].

## 4 Conclusions

The effect of support morphology on the activity for the WGS reaction over copper supported on ceria nanospheres and nanocubes was investigated by using in situ XRD and pulsing one of the reactants (CO). In the presence of CO, CuO is rapidly reduced to Cu<sup>0</sup> and Ce<sup>3+</sup> sites are formed in ceria. The reduction of the copper and cerium cations in the CuO–CeO<sub>2</sub> interface is strongly linked, revealing a synergistic redox partnership between copper and ceria. The

results showed that the activity and stability of the catalyst active phase had a significant dependence on the ceria support morphology, with CuO/CeO<sub>2</sub> (ns) showing the better activity and stability. The differences in the activity were associated with the unique properties of CuO/CeO<sub>2</sub> (ns), such as the easier reduction of highly dispersed CuO to metallic Cu, the higher stability of the formed metallic Cu, and the larger concentration of Ce<sup>3+</sup> in CeO<sub>2</sub> (ns).

**Acknowledgments** The work performed at Brookhaven National Laboratory, was supported by the U.S. Department of Energy, Office of Science, Office of Basic Energy Sciences, and Catalysis Science Program under contract DE-AC02-98CH10886 contract. This work used resources of the National Synchrotron Light Source, which is a DOE Office of Science User Facility. The financial support from the National Natural Science Foundation of China (Grant 21303272) is gratefully acknowledged. Financial support from MINECO (CTQ2012-32928 project) and EU COST CM1104 action is also acknowledged.

## References

- Shinde VM, Madras G (2013) *Appl Catal B Environ* 132–133:28–38
- Zhang Y, Chen C, Lin X, Li D, Chen X, Zhan Y, Zheng Q (2014) *Int J Hydrogen Energy* 39:3746–3754
- Zhao F, Liu Z, Xu W, Yao S, Kubacka A, Johnston-Peck AC, Senanayake SD, Zhang A-Q, Stach EA, Fernández-García M, Rodríguez JA (2014) *J Phys Chem C* 118:2528–2538
- Wang T, Porosoff MD, Chen JG (2014) *Catal Today* 233:61–69
- Roh H-S, Potdar HS, Jeong D-W, Kim K-S, Shim J-O, Jang W-J, Koo KY, Yoon WL (2012) *Catal Today* 185:113–118
- Gayen A, Boaro M, Leitenburg C, Llorca J, Trovarelli A (2010) *J Catal* 270:285–298
- López Cámara A, Monte M, Martínez-Arias A, Conesa JC (2012) *Catal Sci Technol* 2:2436–2439
- Guo R-T, Zhen W, Pan W, Zhou Y, Hong J, Xu H, Jin Q, Ding C, Guo S (2014) *J Ind Eng Chem* 20:1577–1580
- Amin NAS, Tan EF, Manan ZA (2003) *Appl Catal B Environ* 43:57–69
- Laguna OH, Hernandez WY, Arzamendi G, Gandia LM, Centeno MA, Odriozola JA (2014) *Fuel* 118:176–185
- Jeong D-W, Na H-S, Shim J-O, Jang W-J, Roh H-S, Jung UH, Yoon WL (2014) *Int J Hydrogen Energy* 39:9135–9142
- Meher SK, Rao GR (2012) *J Colloid Interface Sci* 373:46–56
- Tana ZM, Li J, Li H, Li Y, Shen W (2009) *Catal Today* 148:179–183
- Yao SY, Xu WQ, Johnston-Peck AC, Zhao FZ, Liu ZY, Luo S, Senanayake SD, Martínez-Arias A, Liu WJ, Rodríguez JA (2014) *Phys Chem Chem Phys* 16:17183–17195
- Hanson JC, Si R, Xu W, Senanayake SD, Mudiyansele K, Stacchiola D, Rodríguez JA, Zhao H, Beyer KA, Jennings G, Chapman KW, Chupas PJ (2014) *Martinez Arias A* 229:64–71
- Lin J, Huang Y, Li L, Wang A, Zhang W, Wang X, Zhang T (2012) *Catal Today* 180:155–160
- Xu W, Si R, Senanayake SD, Llorca J, Idriss H, Stacchiola D, Hanson JC, Rodríguez JA (2012) *J Catal* 291:117–126
- Rodríguez JA, Hanson JC, Wen W, Wang X, Brito JL, Martínez-Arias A, Fernández-García M (2009) *Catal Today* 145:188–194
- Barrio L, Estrella M, Zhou G, Wen W, Hanson JC, Hungria AB, Homes A, Fernández-García M, Martínez-Arias A, Rodríguez JA (2010) *J Phys Chem C* 114:3580–3587

20. Wang X, Rodriguez JA, Hanson JC, Gamarra D, Martinez-Arias A, Fernandez-Garcia M (2005) *J Phys Chem B* 109:19595–19603
21. Gawade P, Mirkelamoglu B, Ozkan US (2010) *J Phys Chem C* 114:18173–18181
22. Luo M, Ma J, Lu J, Song Y, Wang Y (2007) *J Catal* 246:52–59
23. Rao KN, Bharali P, Thrimurthulu G, Reddy BM (2010) *Catal Commun* 11:863–866
24. Pati RK, Lee IC, Hou S, Akhemonkhan O, Gaskell KJ, Wang Q, Frenkel AI, Chu D, Salamanca-Riba LG, Ehrman SH (2009) *ACS Appl Mater Interfaces* 1:2624–2635
25. Wu Z, Li M, Overbury SH (2012) *J Catal* 285:61–73
26. Liu P, Rodriguez JA (2007) *J Chem Phys* 126:164705